Engineering Fracture Mechanics, 128, 2014, p. 189–204

An improved Vickers indentation fracture toughness model to assess the quality of thermally sprayed coatings

N. H. Faisal [1,2]*, R. Ahmed [2], A. K. Prathuru [1], S. Spence [1], M. Hossain [1], J. A. Steel [1]

[1] *School of Engineering, Robert Gordon University, Garthdee Road, Aberdeen, AB10 7GJ, UK*

[2] *School of Engineering and Physical Sciences, Heriot-Watt University, Edinburgh, EH14 4AS, UK*

Abstract

This study presents an improved approach to the quality assessment of thermally sprayed coatings. Measurements were carried out on five different coatings. Since it is the overall extent of surface cracking during Vickers indentation that is indicative of the volumetric damage, the surface crack length was measured, including the radial cracks, edge cracks, and other cracks around the indentation. It is concluded that the proposed model provides a way forward for determining the fracture toughness (K_{1c}) of brittle materials where no radial cracks are developed. An elastic-plastic finite element simulation of the Vickers indentation test was conducted to locate the stress fields.

Keywords: thermal spray coatings; Vickers indentation; fracture toughness (K_{1c}); edge crack model; finite element analysis

* Author to whom correspondence should be addressed; E-mail: N.H.Faisal@rgu.ac.uk; Tel: +44-1224-26 2438

Nomenclature

$a_{1,2}$	Vickers indentation size for half diagonal 1, 2
a	Average Vickers indentation half diagonal size

B	Slope of line
c_1, c_2	Radial crack along Vickers indentation diagonals, $c = l + a$
D	Median crack depth
E	Elastic modulus
h	Palmqvist crack depth
Hv	Vickers hardness number
k_e	Fracture toughness (edge crack) empirical constant
k_L	Fracture toughness (total surface crack) empirical constant
k_m	Fracture toughness (half-penny/radial-median) empirical constant
k_p	Fracture toughness (Palmqvist) empirical constant
k_{total}	Fracture toughness (total crack) empirical constant
K_1	Stress intensity factor (type 1: opening mode)
K_{1c}	Fracture stress (fracture toughness, type 1: opening mode)
l, l_a	Surface radial crack length
l_{yn}	Crack path unit length
L	Total surface crack length
m	Edge crack depth
P	Indentation load
R	Linear correlation coefficient
R_a	Average surface roughness
$x_{1, 2, ..n}$	Serrated crack path unit length
σ_A	Uniform stress field in an infinite plane
σ_I	Indentation stress (dynamic)
σ_R	Residual stress (static)
σ_y	Yield strength

ψ	Empirical constant (stress intensity factor)
v	Poisson's ratio
AE	Acoustic emission
APS	Air plasma spray
FEA/FEM	Finite element analysis/modelling
GE	Generic equation
HVOF	High velocity oxy fuel
XRD	X-ray diffraction

1. Introduction

Although indentation fracture toughness (K_{1c}) is not considered as being reliable measurement in terms of an absolute material value but comparative behaviour can be well reflected by the method. To quantify Vickers indentation cracking and fracture toughness, by far the greatest attention has been directed to the relatively well defined classical crack configurations (e.g. Palmqvist or radial-median). Further to this, the uncertainty in measuring the crack lengths in Vickers indentation fracture test makes empirical toughness models [1] particularly unsuitable for brittle coating materials (e.g. thermal sprayed cermet/ceramic coatings). Irregular networks of smaller cracks not originating at indentation corners (reported as 'no dominant cracks' [2]) have been observed by investigators [2-7] working on thermally sprayed coatings. The empirical models tend to be based on an idealised cracking pattern and do not account for other cracks around indentations. Previously, authors investigated an acoustic emission (AE) based non-destructive technique of characterising the indentation fracture pattern in thermally sprayed coatings with a view to quantitatively evaluate WC-Co coatings [8] and Al_2O_3 coatings [9-10] quality, indentation loading stages based on the AE criteria [11], and AE based analysis of fracture toughness of various cermet

and ceramic coatings [12]. However, in this paper the work has been to establish a non-AE based working mathematical (empirical) model, which is based on measurable total surface crack and total surface crack length but excluding total radial cracks (i.e. edge cracks), to the quality assessment of thermally sprayed WC-Co cermet and Al_2O_3 ceramic coatings. This can provide a way forward for determining the Vickers indentation fracture toughness of brittle materials where crack other than Palmqvist or half-penny/radial-median cracks are developed.

The durability of thermal spray coating for wear and fatigue applications [13-16] is dependent upon a combination of coating and substrate properties including resistance to fracture within the coating (cohesive failure) or at the coating substrate interface (adhesive failure). Fracture toughness of the coating, both parallel and perpendicular to the direction of spraying due to its lamellar microstructure, ability of the substrate to support coating under indentation or contact stress, role of residual stress are some of the key design factors controlling the performance of coated components. A more reliable interpretation of crack patterns used to infer fracture toughness using Vickers test on a given coating substrate system will inevitably improve the design quality of manufactured components. Typical Vickers indentation fracture patterns for thermally sprayed cermet/ceramic coatings consist of a network of cracks around the indentation. As well as this network, radial cracks emanating from the two opposite indent corners, on a plane parallel to the coating-substrate interface, can also be seen. The indentation fracture in these coatings also tends to be asymmetric, which has been attributed to a macroscopic variation in relative density, the presence of pores or other defects around the contact and through thickness residual stresses variation [2]. It has been suggested that indentation in porous regions of the coatings results in localized densification about the contact site, resulting in little transmission of indentation stresses to the surrounding materials, and the confinement of cracking to the vicinity of the impression

[2]. Interaction with large coating pores or defects near the impression diagonal would then be expected to result in longer cracks, producing a modified Boussinesq stress field. Since the degree of porosity varies between coatings (e.g. HVOF < APS [5]) as well as within a given coating, it has been suggested [2] that different loads would be required to produce cracking in different coatings of the same type and even from place to place in a single coating.

Recent investigations [3] give a typical example of the fracture pattern around Vickers indentations in functionally graded HVOF WC-NiCrBSi coating, preferring qualitative analysis to the empirical models as reviewed by Ponton and Rawlings [1] to obtain fracture toughness. They pointed out that, if micro-fissuring in the sub-surface region takes the place of surface radial cracks at lower loads, this complicates the issue of using empirical models to measure fracture toughness. Factor and Roman [4-5] observed both radial and circular cracks in thermally sprayed coatings, but found that most were of mixed characteristic and were not easy to categorise. The uncertainty in measuring the crack lengths in cracking from indentation [4-5] makes empirical fracture models (e.g. Palmqvist or radial-median) unsuitable, in particular for thermal sprayed coatings, and it is expected that an improved method of crack length/fracture toughness measurement may provide an improved solution to this problem.

For stress-free materials (e.g. free from pre-existing residual stress), cracks within point contact elastic stress field (Boussinesq field [17-20]) can initiate from pre-existing flaws [21] or flaws induced by the indentation itself [17-18]. Upon attaining some critical configuration, a dominant flaw develops into a well-defined propagating crack, and tends to propagate along trajectories which maintain near orthogonality to a major component of tension in the Boussinesq field. However, a presence of through thickness pre-existing residual stress field [9-10, 20] in a coating-substrate system can strongly affect the coatings failure [2-3, 9-10]. There is no simple relationship between cracking pattern and total stress distribution during

indentation, but combined dynamic indentation stress ($\pm\sigma_I$) and pre-existing static residual stress ($\pm\sigma_R$) can affect the indentation response of materials significantly [19-20, 22-24]. To model more complex indent shapes, such as those produced by the Vickers indenter requires a numerical approach, such as finite element analysis [25-26].

Despite some theoretical limitations (e.g. considering elastically deformable material, ignoring surface roughness, and taking coating and substrate as solid and homogeneous materials), Baung *et al.* [25] simulated Vickers indentation on HVOF coatings to determine the stress distributions and critical loads in the coating/substrate systems, relating their findings to the observed cracking profile. It has been indicated by Baung *et al.* [25] that the highest compressive stress occurs in the area right beneath the indenter tip and the highest tensile stress occurs in the centre of the indentation edges and decreases along the indentation edge towards the indentation corner. This suggests that edge cracks will initiate first at the coating surface, and will propagate along the indentation edge. Also, the high tensile stress in the area of the indentation corners induces corner cracks to propagate radially outwards along the diagonal of the indentation.

In this study the focus has been the surface cracking patterns developed in HVOF and APS cermet/ceramic coatings leading to an improvement in conventional approach to assess the Vickers indentation fracture toughness. This also includes supplementing the coating failure locations with the finite element (FE) stress distribution during Vickers indentation.

2. Experiments and simulations

2.1. Specimens and characterisation

As listed in Table 1, five different types of thermally sprayed coating materials were chosen, each coating having a variation in the deposition conditions and/or post-deposition treatment. The coatings which were prepared onto one side of a substrate consisting of an

AISI 440C martensitic stainless steel disc of diameter 31 mm and thickness 8 mm using industrially optimized conditions [12, 27]. These coating materials were chosen to give a range of accommodation mechanism from combined plastic deformation and brittle fracture e.g. in cermets (all three WC-Co coatings), to fracture with little or no plastic deformation in ceramics (both Al_2O_3 coatings). In preparation for the indentation tests, specimens surface were ground and polished using diamond paste to avoid any effect of polishing which was expected to be broadly similar for all coated specimens [8-12, 27-29].

The microstructure of the specimens and the indentations were examined using an optical microscope (Nikon, with N50 monochrome camera), at various magnifications and, where necessary, using a Scanning Electron Microscope (Hitachi: S-2700 and Philips: XL30). In the SEM images (Fig. 1a), the polished surfaces are quite smooth, with a homogeneous microstructure and little surface connected porosity. The carbide particles are relatively angular. The WC-12%Co (JetKote) coating microstructure was not distinguishable from the WC-12%Co (JP5000) coating, hence not shown in Fig. 1. The HIPed WC-12%Co (JetKote) microstructure was relatively denser than as-sprayed, hence not shown in Fig. 1. The SEM images of APS Al_2O_3 coatings (Fig. 1b) show that the molten Al_2O_3 droplets have spread significantly and it is not possible to distinguish any non molten or semi molten particles. A Bruker AXS, Model D8 ADVANCE X-Ray diffractometer was used operating at 40 kV and 40 mA. Cu-$K\alpha$ radiation was used (wavelength, $\lambda = 0.1542$ nm) and the goniometer was run from 5° to 90° with a step size of 0.009° (2θ) at 15.4 seconds per step. X-ray diffraction (XRD) analysis (Table 1) was used to identify the crystalline phases present in the coatings. The Vickers microhardness was obtained (Table 1) using a calibrated Mitutoyo, MVK-H1 machine for five indentations applied to the surface of specimens at 1.96 N (or HV0.2) load.

2.2. Vickers indentation measurements

Using a calibrated machine five indentations were carried out at each of the indentation loads (49, 98, 147, 196, 245, 294, 343, 392, 441 and 490 N for all three WC-Co based cermet coatings and 98, 147, 196, 245, 294, 343, 392, 441 and 490 N for both Al_2O_3 ceramic coatings). The duration of the application of the test force was 15 seconds. Indentations were spaced greater than 2.5 times the diagonal apart [30], to avoid any interaction between the surface and sub-surface fractures of neighbouring indentations [8, 27].

The conventional method of measuring the crack length (using a direct straight-line method [1]) around indentations simply determines the average diagonal size (including radial cracks, 2*c*) and subtracts half the average impression diagonal size $a = (2a_1 + 2a_2)/4$, so that l_a, the average of the radial crack lengths at the four indent corners, is given by: $l_a = c - a$. Because the cracks were branched in all cases, a profiling method [8, 12, 27] was used in this study as shown in Fig. 2. Accordingly, the surface crack length was measured, including radial cracks at corners, edge cracks, ring-shaped cracks and other small cracks around the indentation as shown in the schematic diagram in Fig. 2. As illustrated in Fig. 2, crack lengths in the surface plane between points A and B were assessed using a profiling method by adding together the serrated crack path unit lengths, $l_{yn} = x_1 + x_2 + ... + x_{n-1} + x_n$. The minimum unit length was determined by the resolution of the micrograph (here 2 - 3 μm). The total surface crack length was then obtained from the sum of all the *n* resolvable crack lengths using equation (1):

$$L_{total} = \sum_n l_{yn} \qquad (1)$$

Also, for comparison with conventional approaches, l_a, the average of radial crack lengths at the four indent corners was determined and the dimension, *c*, calculated from equation (2) [1]:

$$c = l_a + a \qquad (2)$$

Other sub-surface cracks [8, 12, 27] which are not measurable using the optical microscope without sectioning and are therefore not included in the above technique. Surface crack length measurements were made on an optical microscope at various magnification levels appropriate to the size of indentation.

In this work, the analysis has been based on two main classical models (Palmqvist and half-penny/radial-median [1]) and also an alternate approach based on total surface crack length and total surface crack length excluding total surface radial cracks. According to the various published analyses of the indentation of brittle materials, Nihara *et al*. [31] have distinguished between the two in terms of the classical dimensions a, l_a and c: Palmqvist cracks, $l_a/a \leq 2.5$ or $c/a \leq 3.5$ and half-penny cracks, $c/a \geq 2.5$ [32-34]. In the current study, the average value of l_a/a and c/a were well within the Palmqvist régime, and this was also supported by the absence of sub-surface radial-median cracks [8, 27]. Shetty *et al.* [35] have devised an empirical model for Palmqvist cracks, which allows the fracture toughness (in units MPa.m$^{1/2}$) of the coating to be determined from the load and crack dimensions:

$$K_{1c} = 0.0319\left[\frac{P}{a\sqrt{l_a}}\right] \qquad (3)$$

where P is the indentation load (in Newtons), a is the average indent half-diagonal size and l_a is the average of the radial corner crack lengths, both in metres.

The above formula for the determination of fracture toughness assumes that the surface is initially stress-free (e.g. residual stress). Ponton and Rawlings [1] reviewed and developed a series of generic fracture toughness equations, to describe the relationship between the surface radial crack length, l, indent half diagonal, a, and indentation load, P. They recommended 'generic equations' (GEs) which summarise much of the practice observed, but all essentially use a crack length measurement and, implicitly utilise the relationship $K_I = \psi\sigma_A\sqrt{c}$ [18]. In this work, the GE has been modified (equation 4) to replace the average

radial-corner crack length l_a, with the total surface crack length L to give a modified generic equation for total surface crack length-based fracture toughness estimation (K_{1c}) for Palmqvist type cracks:

$$K_{1c} = k_L\left[\frac{P}{a\sqrt{L}}\right] \quad (4)$$

where a and L are in meters, k_L is an empirical constant which can be determined for any given indenter/specimen/indentation system combination. All above experimental data including indentation tests were collected at room temperature.

2.3. Finite element modeling of Vickers indentation

To study the materials failure in the coating-substrate system under Vickers indentation and association with the stress fields, a three-dimensional FE (elastic-plastic) model was developed using ANSYS (14.0) Mechanical APDL package. This model does not account for the presence of residual stress in the coating-substrate system, friction during indentation contact and indentation induced cracking. Due to the geometrical and loading symmetry, the model was generated for a quarter of a pyramidal shape indenter (Vickers, Fig. 3) loaded on the coated surface, corresponding to an indentation test load of 490 N. The model includes a deformable-diamond indenter and a deformable-coated specimen on the substrate. The maximum principal stress field was determined and compared with the cracking features observed in the experimental results. Although the FE model does not include any defects within materials and assumes residual stress (pre-existing) free coating perfectly bonded to the substrate, it provides an estimate of the elastic-plastic stress distribution to mimic the experimental results. The system geometry and constraints are shown in Fig. 3(a) and material properties are listed in Table 2 for the indenter, coatings and substrates. As listed in Table 2, three separate FE simulations were investigated which includes WC-12%Co, APS Al_2O_3 and HVOF Al_2O_3 coatings. All coatings and substrates were considered solid and

homogeneous. The coating thickness and the elastic modulus listed are all measured values listed in Tables 1 and 2. An upper bound value of AISI 440C steel substrate yield strength (σ_y = 1.28 GPa) was selected on the basis of literature [36] while using appropriately calculated yield strength [37] ($\sigma_y = 3.5Hv$, where Hv is measured values as shown in Table 1) values for each coatings listed in Table 2. A frictionless contact is applied between the bottom edge of the indenter and the top edge of the coating. The load is applied to the central vertical edge of the indenter. The meshes used are hexahedral in the coating and substrate and tetrahedral in the indenter. The element sizes are gradually reduced toward the indentation region in order to refine the solution. As an example, the Fig 3(b) shows the mesh for the 3D model of the WC-12%Co coating with the AISI 440C steel substrate.

3. Results and discussion

3.1. Vickers indentation cracking features

In the coating materials investigated, accommodation is by crumbling of the surface to the extent that cracking cannot be entirely identified by metallographic means [8-12, 27]. As expected in brittle thermally sprayed coating materials [8-12, 27], material accommodation such as 'sinking-in' can be identified for all coatings. Based on the surface micrographic observations of the indentations on the various coatings, the probable residual impression of cracking after an indentation can be summarised with representative examples in Fig. 4. Three distinct cracking patterns around indentations can be seen for the coatings considered in this investigation. The surface fracture pattern includes radial cracks at the four corners, edge cracks (or edge chipping), ring cracks and other small cracks around the indentation.

Figure 4 shows typical Vickers indentation cracking patterns of coatings at all of the loads (examples shown here for 441 N load) except at the lowest load of 49 N. For the as-sprayed HVOF (JP5000 and JetKote) WC-12%Co coatings (e.g. Fig. 4a), radial cracking from all or

any of the four corners of the indentation was seen for loads of 98 N upwards. At the lowest load of 49 N, only minor cracks around the perimeter (edge cracks) and on the surface of the indentation were found. The indentations of HIPed HVOF (JetKote) WC-12% Co coating (Fig. 4b) showed only edge cracks and other small cracks around the indentation with no visible radial cracking for any of the indentations at any of the loads.

The indentations of the APS Al_2O_3 (conventional powder) coatings (Fig. 4c) showed a significant degree of crushing fracture and spallation and very different to all the other coating examples. Due to meshed cracks and spalled asymmetrically features around indentations, it was not possible to experimentally measure the crack lengths either using the direct straight line or profiling method for the APS Al_2O_3 coatings. The indentations of HVOF Al_2O_3 (fine powder) coating showed (Fig. 4d) visible radial cracking from all four corners at all loads, and the surface fracture pattern included edge cracks around the indentation.

The indentation induced failure features in APS Al_2O_3 coatings tends to be highly asymmetric, which can be attributed to macroscopic variation in relative density, the presence of pores or other defects around the contact and through thickness pre-existing residual stresses variation [2]. It has been suggested that indentation in porous regions of the coatings results in localized densification about the contact site, resulting in little transmission of indentation stresses to the surrounding materials, and the confinement of cracking to the vicinity of the impression [2]. Interaction with large coating pores or defects near the impression diagonal would then be expected to result in longer cracks, producing a modified (Boussinesq [17-20]) stress field.

Recently, the authors have investigated through-thickness pre-existing residual stress (static stress) profile in both Al_2O_3 coating materials using neutron diffraction [e.g. 9-10]. Since indentation pressure is compressive just below the indenter tip and perpendicular to the

applied surface, the existence of pre-existing tensile residual stress (relatively higher for APS Al_2O_3 coating [9-10] in the surface will increase the magnitude of shear stress leading to surface failure beneath the indenter as was seen in the form of localized mesh and spallation [2, 6] for APS Al_2O_3 coating (Fig. 4c). However, relatively less pre-existing tensile residual stress in the surface for HVOF Al_2O_3 coating [9-10] reduced the coating failure in the form of localized mesh and spallation, dominating the effect of indentation elastic stress field failure, as was seen (Fig. 4d) in the form of typical corner radial and edge cracking [3, 8-12, 27]. Attenuation in the through-thickness pre-existing residual stress profile also plays an important role in the cracking propagation and suppression [28-29], and it has been observed that at the same Vickers indentation load, the relatively high pre-existing residual compressive stresses in HIPed coatings (e.g. HVOF WC-NiCrBSi) [28] inhibited the extension of cracks seen in the as-sprayed coating [3]. Therefore, relatively less cracks around indentation for HIPed HVOF (JetKote) WC-12%Co coatings in the current investigation can also be expected.

3.2. Vickers indentation crack length indicator

All cracks visible were measured (Fig. 5) according to the scheme described in *Section 2.2*. The cracking features of indentation surface and their prevalence are summarised in Table 3. Clearly, in the coatings material studied, the cracking behaviour is generally much more complex than is assumed for either the classical models of Palmqvist (Nihara [33]) or radial-median (Lawn and Fuller [34]) cracking. There is no simple relationship between hardness and cracking pattern (Table 3), although the amount of cracking is probably related to toughness and its distribution depends both on toughness and homogeneity [11, 27]. In the hard, multi-phase materials, inhomogeneity means that the areas of highest fracture toughness do not always correspond to the areas where cracking occurs and the size and distribution of

the phases, their respective K_{1c} values, and the existence of brittle surfaces (e.g. splat boundaries) will all influence the cracking pattern. It can be observed (Table 3) that the ranking of the prevalence of radial cracking is in the similar order to the ranking of the prevalence of edge cracking and total surface cracking.

3.3. Vickers indentation fracture toughness assessment

In order to obtain the fracture toughness data as a function of indentation geometry and crack length, the indentation test method has been applied. Figure 6a shows the basis of the classical approach to Vickers indentation fracture toughness measurement where one of the two assumptions is made about the sub-surface shape of radial cracks: (a) in the first approach (Nihara [33]), the length of each radial crack is taken to be visible length, l, and the depth, h, is assumed to be proportional to the impression depth, which leads to a relationship between fracture toughness, crack size, load and impression size, $K_{1c} = k_p\left[\frac{P}{a\sqrt{l_a}}\right]$, and (b) in the second approach (Lawn and Fuller [34]), the radial cracks are assumed to form part of a single crack whose length ($2c$) includes the impression diagonal and where depth (D) is half the length. This leads to proportionality, $K_{1c} = k_m\left[\frac{P}{c^{3/2}}\right]$.

In order to obtain the fracture toughness data as a function of indentation geometry and edge crack length, the indentation test method has been proposed, as shown in Fig. 6b, which is an extension of the fracture mechanics model for 'edge cracks'. Using the classical crack régimes in Vickers indentation fracture tests, the average crack-to-indent ratio (l_a/a around 0.43±0.08 for as-sprayed HVOF/JetKote WC-12%Co, 0.45±0.08 for as-sprayed HVOF/JP5000 WC-12%Co; 0.88±0.21 for HVOF-theta gun Al_2O_3 fine powder), suggests Palmqvist rather than median cracks, and this is supported by the absence of sub-surface radial-median cracks in the SEM images of as-sprayed HVOF (JetKote) WC-12%Co [8, 27].

Hence, it is reasonable to assume that similar mechanics hold for edge cracks with stress being dependent upon the load and penetration depth. Using a similar assumption to the Palmqvist model (i.e. that crack depth, *m*, is proportional to impression size), the toughness can be deduced to be given by $K_{1c} = k_e \left[\frac{P}{a\sqrt{\sum l_{yn}}} \right]$. There is no reason to suppose that $k_e = k_p$ but, for combination of edge and radial cracks, the relationship between load and total surface crack length can still be considered to be an indication of fracture toughness.

Figure 7 presents two approaches in Vickers indentation fracture toughness assessment which includes classical and alternative approach. Figure 7a presents the application of classical (Palmqvist model) average radial crack length approach (which exhibited any radial cracking). Using the classical constant of proportionality, $k_p = 0.0319$ (e.g. Shetty *et al.* model [35]), a value of fracture toughness can be obtained for the as-sprayed HVOF (JetKote) WC-12%Co and as-sprayed HVOF (JP5000) WC-12%Co coatings as 8.8±0.5 MPa.m$^{1/2}$ and 9.1±1.0 MPa.m$^{1/2}$, respectively. For the same coating material (WC-12%Co as-sprayed HVOF/Diamond Jet METCO), Lima *et al.* [38] have determined a value of 5.1±0.7 MPa.m$^{1/2}$ (Palmqvist based Shetty *et al.* model [35]) and 4±1 MPa.m$^{1/2}$ (Palmqvist based Nihara model [33]), although it might be noted that their indentations were made on a cross-section of the sample (as opposed to on its surface) and the fracture toughness for sprayed coatings is known to be anisotropic [38-40]. Considering the Palmqvist model, the fracture toughness for the HVOF-theta gun Al_2O_3 (fine powder) coatings studied here was 5.5±0.5 MPa.m$^{1/2}$. For a similar coating (HVOF Al_2O_3, powder size unknown), Bolelli *et al.* [41] have given a value of 2.5±0.57 MPa.m$^{1/2}$, although they did not indicate the direction of indentation and what fracture model they used. For APS (Metco 9MB) Al_2O_3 (conventional powder) coating, where a measurement of K_{1c} was not possible in this work, Bolelli *et al.* [41]

have given a value of 2.33±0.36 MPa.m$^{1/2}$, although, again, powder size, indentation direction and fracture model were not specified.

Figure 7b shows the application of a combined radial and edge crack model to all of the coatings studied (except the APS Al_2O_3). The plot in Fig. 5b shows the relationship between total surface crack length and total surface edge crack length and, as can be seen, the ratio (total-crack : edge-crack) varies between unity and about 2. The plot of $a\sqrt{L}$ against *P* yields a straight line (Fig. 7b) from which the fracture toughness can be determined. For the k_{total} to be comparable with the value of k_p for Palmqvist cracks (the coefficient k_{total} is multiplied by 2), it is necessary to divide the total crack length by 4 (in order to normalise per edge or per corner in Vickers indentation) and Table 4 shows the resulting values of K_{1c} using edge and radial cracks (where these exists) and edge cracks only. The alternative approach does not change the ranking of fracture toughness between the three WC-Co based coatings and gives values that are rather more compatible with the literature values discussed above.

In the absence of radial cracks for the HIPed HVOF (JetKote) WC-12%Co coating (HIPed expected to be tougher over as-sprayed coatings [28-29]), the classical approach (Palmqvist or radial-median/half-penny models) cannot be used. However, the alternative approach (edge crack model) gives a value of 7.4 MPa.m$^{1/2}$ compared with 4.6-5.2 MPa.m$^{1/2}$ for the equivalent as-sprayed coatings. The complexity in measuring the typical radial crack lengths in APS Al_2O_3 coatings has also been commented on by Luo *et al.* [6] and Sharma *et al.* [42]. However, the results shown here indicate that total surface crack length (significant in APS Al_2O_3) can be used to qualitatively rank the fracture toughness in such coatings.

3.4. Finite element analysis of Vickers indentation

Because of their complex nature, including properties which vary with depth and multiphase mixture of materials of varying toughness [2, 4-5, 9-12, 27-29], FE simulation of

indentation testing of thermally sprayed coatings can provide valuable information to ascertain the dominant stress fields. However, this model does not account for the presence of residual stress, contact friction and indentation cracking, but it is known that for fracture in brittle materials, maximum principal stress is the main consideration. Therefore, in the current investigation the main focus has been the cracking patterns developed in HVOF and APS ceramic coatings and comparing it with the maximum principal stress using FE Vickers indentation.

According to the indentation test results, the WC-12%Co, APS Al_2O_3 and HVOF Al_2O_3 specimens fractured at all loads investigated. The FE maximum principal stress results are presented for maximum test load of 490 N (Fig. 8). The ability of substrate (yield strength) to support the coating plays an important role in combating coating failure during Vickers indentation as it alters the material accommodation mechanism. Under contact stress conditions previous investigations have highlighted that the failure mechanism of coating can shift from coating delamination to bulk coating failure at lower values of substrate yield strength [14-16]. Figure 9 presents the schematic of the Vickers indentation impression and the key stress location analysed and summarised in Fig. 10. It has been indicated for elastic coating and elastic-plastic substrate FE model [25] the highest compressive stress occurs in the area right beneath the indenter tip and the highest tensile stress occurs in the centre of the indentation edges (wider at the centre of the edge) and decreases along the indentation edge towards the indentation corner. However, in the current elastic-plastic model, the highest compressive stress occurs in the area right beneath the indenter tip (directional variation can be seen in Figs. 10a,b) but the highest tensile stress occurs at a certain distance from the indentation corner along the radial direction, and the next highest tensile stress occurs at a certain distance in the centre of the indentation edges and decreases along the indentation edge towards the indentation corner until it crosses the highest tensile stress area at the

indentation corner (Fig. 10c). This suggests that radial cracks will initiate first at the coating surface near the indentation corner, and will propagate along the diagonal of the indentation. Also, the high tensile stress in the area of the indentation edge induces edge cracks to propagate along the indentation edge. The experimental results (e.g. the residual impression of Vickers indentation) on various coatings (Fig. 4) can be compared with the FE simulation results for maximum principal stress distribution (Fig. 10).

For the three coatings investigated through FE simulations at 490 N load, the distance to the observed highest stress (tensile) varies which occurs around the indentation corner just outside the contact area along the diagonal direction (X_2X_3). As can be clearly seen in Fig. 10a, as the elastic modulus decreases ($E_{WC\text{-}12\%Co}$ = 231 GPa; $E_{APS\ Al2O3}$ = 180 GPa; $E_{HVOF\ Al2O3}$ = 170 GPa), the location along OX_2X_3 of the highest stress (tensile) at about X_2 shifts towards X_3 (also the highest tensile stress values decreases with the decrease in elastic modulus). Also, it can be clearly seen in Fig. 10b, as the elastic modulus decreases, the location along OE_cO' of the high stress (tensile) at about indentation edge centre (E_c) shifts towards O'.

These simulation results summarised in Fig. 10 provide two key theoretical foundation for the cracking (or crack initiation) of coating materials under the Vickers indentation. Firstly, as observed in Fig. 10a, the distribution of the maximum principal stress (tensile) presents the highest stress at a certain distance (different for each coating) from the indentation corner for the coating materials investigated. Therefore, the cracks can be induced initially at the indentation corner (due to tensile stress) and propagated along the indentation corner radial direction, also observed in the experimental results (Fig. 4). Secondly, the simulation results (Fig. 10b) also indicated that the maximum principal stress is high (also tensile), which can explain why the edge cracks would appear. Comparing the values of maximum principal

stress at the indentation edge and at the corners, it can be observed that the corner crack was initiated first and the edge crack was induced with further increment in loading.

For the 490 N indentation load (Fig. 10a), at the corner of the indentation the maximum principal stress are about 2.4 GPa for WC-12%Co, 2.2 GPa for HVOF Al_2O_3 and 2.3 GPa for APS Al_2O_3 coating materials; therefore, the radial cracking are more dominant for WC-12%Co (as-sprayed JP5000) coatings. Interaction with large coating pores (e.g. APS Al_2O_3) or low coating pores (e.g. HIPed WC-12%Co), or degree of porosity between coatings as well as within a given coating, or defects near the impression diagonal would then be expected to result in longer (or shorter or none) cracks, producing a modified stress field.

For the 490 N indentation load (Fig. 10b), at the centre of the indentation edge the maximum principal stress are about 1.06 GPa for WC-12%Co, 1.15 GPa for HVOF Al_2O_3 and 0.62 GPa for APS Al_2O_3 coating materials. Since these values are larger than the tensile strength of these derivative materials (e.g. 0.2 GPa for WC hard metal [43], 0.26 GPa for Al_2O_3 ceramic [44]); therefore, the cracking are all over the indentation edge.

The Vickers indentation FE simulated depth at 490 N load calculated was 119 μm (Fig. 10a) which is almost double the experimentally measured depth (e.g. 66 μm for as-sprayed HVOF JP5000 WC-12%Co coating [11]) and this could be due to elastic-plastic model considered for both coating and substrate. However, considering elastic model, the Vickers indentation FE simulated depth at 490 N load calculated was 61 μm which is close to the experimental measured depth.

As discussed above, the indentation contact stress fields can be useful in indicating how indentation response (deformation and cracking) will tend to initiate at the surface, subsurface level and at the coating-substrate interface. This is in order to understand the possible effect of substrate deformation during indentation on developed crack pattern and the calculation of fracture toughness. The lower indentation loads on the coating surface was

expected to induce very little or no strain mismatch at the coating-substrate interface and it may not be easy to observe subsurface cracks. However, other form of cracks (e.g. near surface cracking and delamination) can be observed [8]. It should be noted that mismatch in the coating and substrate properties (e.g. hardness, elastic modulus) also influence the extent of coating failure [14-16]. The effect of the coating on the substrate deformation can be neglected where the indentation depth is considerably lower than the thickness of the coating. Although the application of higher loads on the coating surface was expected to induce significant strain mismatch in the coating-substrate system (leading to cohesive and adhesive failure) both during loading and unloading, there are very little investigations in literature to consider this aspect of research in thermal spray coatings. At higher loads, the yielded substrate may not provide support the coating and this can be decisive for cracks initiation and their propagation. However, it has been indicated [4-5, 8, 19, 39, 42, 45-47] that the dominant material accommodation mechanisms in non-homogeneous materials like thermally sprayed coatings are cracking at inter-splat boundaries and also material densification due to the collapse of porosity within the coating microstructure, and qualitative or quantitative evaluation of fracture toughness of coating material is possible using other technique (e.g. acoustic emission [12, 19]) at variety of loads.

There is no simple relationship between the structure of a coating and its influence on degradation and failure during its potential applications [48-51]. However, this work provides an ability to relate the role of structure–property relationships to degradation and failure, which otherwise would be difficult to ascertain using conventional empirical techniques. Despite some theoretical limitations (e.g. considering elastic-plastic deformable material, ignoring surface roughness, and taking coating and substrate as solid and homogeneous materials), the FE simulations of Vickers indentation on coating-substrate systems presents a good summary of the experimental findings related to the observed cracking profile.

4. Conclusions

The main conclusions drawn are as follows:

i. The ranking of the prevalence of radial cracking is in similar order to the ranking of the prevalence of edge cracking and total surface cracking. This can be used as a way forward using the edge or total cracking for fracture toughness measurement.

ii. The empirical models (Palmqvist or half-penny/radial-median) tend to be based on an idealised cracking pattern and do not account for other cracks around indentations. The proposed model using the total surface crack and total surface crack length excluding total surface radial cracks (e.g. edge cracks) can provide a way forward for determining the Vickers indentation fracture toughness of brittle materials, where crack other than Palmqvist or half-penny/radial-median cracks are developed. These fracture toughness values are in good agreement with the few available published values. Using total surface crack length excluding total surface radial cracks approach, the following values are suggested:

   4.3±0.1 MPa.m$^{1/2}$ for HVOF (theta-gun) Al_2O_3

   5.2±0.3 MPa.m$^{1/2}$ for as-sprayed HVOF (JetKote) WC-12%Co

   7.4±0.5 MPa.m$^{1/2}$ for as-sprayed HVOF (JP5000) WC-12%Co

   7.4±0.2 MPa.m$^{1/2}$ for HIPed HVOF (JetKote) WC-12%Co coatings

iii. The finite element stress analysis of Vickers indentation on coating-substrate systems gives a good indication of experimental findings to the observed cracking locations and profiles. The area around the indentation corner shows highest tensile stress, which induced the corner crack and caused the crack to propagate radially along the diagonal of the indentation (predominantly in both as-sprayed WC-12%Co and HVOF Al_2O_3 coatings). The next highest tensile stress occurs at the centre of the indentation

edge and the stress decreases along the indentation edge toward the indentation corner, which induced the edge cracking first in the coating surface and promoted the edge crack growing along the indentation edge (predominantly in both as-sprayed and HIPed WC-12%Co and HVOF Al_2O_3 coatings).

Acknowledgement

The authors would like to thank Deloro Stellite Ltd., UK for supplying the WC-12%Co coated specimens for this study. Thanks are due to J. Kitamura and S. Osawa, Thermal Spray Materials Department, Fujimi Incorporated, Japan for thermal spraying the Al_2O_3 specimens. The authors are also grateful to the IDEAS research institute at the Robert Gordon University for funding the simulation work.

References

[1] Ponton CB, Rawlings RD (1989) Mater Sci Technol 5:865-872

[2] Ostojic P, McPherson R (1987) Mater Forum 10:247-255

[3] Stoica V, Ahmed R, Itsukaichi T, Tobe S (2004) Wear 257:1103-1124

[4] Factor M, Roman I (2002) J Therm Spray Technol 11:482-495

[5] Factor M, Roman I (2002) J Therm Spray Technol 11:468-481

[6] Luo H, Goberman D, Shaw L, Gell M (2003) Mater Sci Eng A 346:237-245

[7] Roman A, Chicot D, Lesage J (2002) Surf Coat Technol 155:161-168

[8] Faisal NH, Steel JA, Ahmed R, Reuben RL (2009) J Therm Spray Technol 18:525-535

[9] Ahmed R, Faisal NH, Paradowska AM, Fitzpatrick M (2012) J Therm Spray Technol 21:23-40

[10] Ahmed R, Faisal NH, Reuben RL, Paradowska AM, Fitzpatrick M, Kitamura J, Osawa S (2010) **J Phy: C S 251, art no.** 012051 (4pp)

[11] Faisal NH, Reuben RL, Ahmed R (2011) Meas Sci Technol 22, art no. 015703 (18pp)

[12] Faisal NH, Ahmed R (2011) Meas Sci Technol 22, art no. 125704 (20pp)

[13] Stoica V, Ahmed R, Itsukaichi T (2005) Surf Coat Technol 199:7-21

[14] Osawa S, Itsukaichi T, Ahmed R (2004) International Thermal Spray Conference (ITSC2004), Osaka, Japan, ISBN 3-87155-792-7

[15] Stoica V, Ahmed R, Golshan M, Tobe S (2004) J Therm Spray Technol 13:93-107

[16] Ahmed R, Hadfield M (2002) J Therm Spray Technol 11:333-349

[17] Lawn BR, Wilshaw R (1975) J Mater Sci 10:1049-1081

[18] Lawn BR (1993) Fracture of Brittle Solids. Cambridge Solid State Science Series, Cambridge, UK

[19] Faisal NH, Ahmed R, Reuben RL (2011) Inter Mater Rev 56:98-142

[20] Faisal NH, Ahmed R (2011) Recent Patents on Mechanical Engineering 4:138-152

[21] Griffith AA (1920) Phil Trans Roy Soc A 221:163-198

[22] Bull SJ (2005) J Phys D: Appl Phys 38:R393-R413

[23] Chen X, Yan J, Karlsson AM (2006) Mater Sci Eng A 416:139-149

[24] Jungk JM, Boyce BL, Buchheit TE, Friedmann TA, Yang D, Gerberich WW (2006) Acta Mater 54:4043-4052

[25] Buang AP, Liu R, Wu XJ, Yao MX (2008) J Coat Technol Res 5:513–534

[26] Cai X (1992) J Mater Sci Lett 11:1527-1531

[27] Faisal NH (2009) Acoustic emission analysis for quality assessment of thermally sprayed coatings. PhD thesis, Heriot-Watt University, Edinburgh, UK

[28] Ahmed R, Yu H, Stoica V, Edwards L, Santisteban JR (2008) Mater Sci Eng A 498:191–202

[29] Ahmed R, Yu H, Stewart S, Edwards L, Santisteban JR (2007) ASME J Tribol 129:411-418

[30] ASTM (1992) Standard test method for Vickers hardness of metallic materials ASTM E 92-82

[31] Nihara K, Morena R, Hasselman DP (1982) J Mater Sci Lett 1:13-16

[32] Liang KM, Orange G, Fantozzi G (1990) J Mater Sci 25:207-214

[33] Nihara K (1983) J Mater Sci Lett 2:221-223

[34] Lawn BR, Fuller ER (1975) J Mater Sci 10:2016-2024

[35] Shetty DK, Wright IG, Mincer PN, Clauer AH (1985) J Mater Sci 20:1873-1882

[36] http://www.matweb.com/

[37] Busby JT, Hash MC, Was GS (2005) J Nuclear Mater 336:267-278

[38] Lima MM, Godoy C, Avelar-Batista JC, Modenesi PJ (2003) Mater Sci Eng A 357:337-345

[39] Cantera EL, Mellor BG (1998) Mater Lett 37:201-210

[40] Babu PS, Basu B, Sundararajan G (2008) Acta Mater 56:5012-5026

[41] Bolelli G, Lusvarghi L, Varis T, Turunen E, Leoni M, Scardi P, Azanza-Ricardo CL, Barletta M (2008) Surf Coat Technol 202:4810-4819

[42] Sharma AK, Aravindhan S, Krishnamurthy R (2001) Mater Lett 50:295-301

[43] Lu SP, Kwon OY (2002) Surf Coat Technol 153:40-48

[44] Munro RG (1997) J Amer Ceram Soc 80:1919-1928

[45] Senturk U, Lima RS, Lima CRC, Berndt CC (2000) Trans. ASME, J. Eng. Gas Turb. Power 122:387-392

[46] Ajit Prasad SL, Mayuram MM, Krishnamurthy R (1999) Mater Lett 41:234-240

[47] Vijayakumar K, Sharma AK, Mayuram MM, Krishnamurthy R (2002) Mater Lett 54:403-413

[48] Chen J (2012) *J Phys D: Appl Phys* 45, art no. 203001

[49] Chen J**,** Bull SJ (2011) *J Phys D: Appl Phys* 44, art no. 034001

[50] Houdkova Š, M. Kašparova M (2013) Engng Fract Mech 110:468-476

[51] Demidova NV, Wu XJ, R. Liu R (2012) Engng Fract Mech 82:17-28

Table captions

Table 1 Coated test specimens for Vickers indentation.

Table 2 Input parameters for finite element simulations.

Table 3 Summary of qualitative and quantitative indentation cracking features.

Table 4 Summary of classical and alternative approach fracture toughness of coatings.

Figure captions

Fig. 1 SEM images of coatings surface morphology: (a) as-sprayed HVOF (JP5000) WC-12%Co. (b) APS (Metco/9 MB) Al_2O_3

Fig. 2 Scheme for measuring the total surface crack length using profiling method. The scheme shown on the left side is applicable for all type of cracks around the indentation [ref. 12]

Fig. 3 Scheme for 3D elastic-plastic finite element modelling using ANSYS (14.0) Mechanical APDL: (a) constraints and loading conditions, and (b) meshing shown here for WC-12%Co coating on AISI 440C steel substrate

Fig. 4 Typical Vickers indentation cracking patterns of coatings at 441 N load: (a) as-sprayed (JP5000) WC-12%Co. (b) HIPed (JetKote) WC-12%Co. (c) APS (Metco/9 MB) Al_2O_3. (d) HVOF (theta-gun) Al_2O_3

Fig. 5 Two approaches in Vickers indentation crack length indicator for fracture toughness assessment: (a) crack length indicator-1 (classical approach). (b) crack length indicator-2 (alternative approach). The error bars indicate the standard deviation of the data

Fig. 6 Schematic diagrams of Vickers indentation residual impression for crack prone materials: (a) Plamqvist and half-penny models by Nihara [adapted from ref. 33] and Lawn and Fuller [adapted from ref. 34]. (b) edge crack model

Fig. 7 Two approaches in Vickers indentation fracture toughness assessment: (a) crack length indicator-1 (classical approach). (b) crack length indicator-2 (alternative approach). The error bars indicate the standard deviation of the data

Fig. 8 Vickers indentation maximum principal stress at 490 N load for coatings: (a) WC-12%Co, (b) APS Al_2O_3, and (b) HVOF Al_2O_3 [Stress unit in MPa]

Fig. 9 Schematic of Vickers indentation impression (adapted from ref. [25])

Fig. 10 Comparison and variation of the Vickers indentation maximum principal stress at 490 N load for coatings along various paths and depths: (a) path OX_2X_3, (b) OE_cO', and (c) E_cX_2

Table 1 Coated test specimens for Vickers indentation.

No.	Coating materials / Spraying gun and type	Thermal spray process parameters	Coating thickness (µm)	Polished surface roughness (Ra, µm)	Microhardness (HV0.2)	XRD phases
Cermet coatings						
1	As-sprayed WC-12%Co/HVOF, JP5000	Powder: WC-12%Co (sintered and crushed, size: 15-50 µm), Oxygen flow: 940 l/min, Kerosene flow: 0.37 l/min, Spray distance: 380 mm,	300-325	0.043±0.01	1002±159	WC phase with some of the harder secondary phase W_2C and a very small amount of metallic W
2	As-sprayed WC-12%Co/HVOF, Jet-kote	Powder: WC-12%Co (sintered and crushed, size: 15-50 µm), Spraying process parameters are not available due to propriety reason.	300-325	0.045±0.03	1050±70	WC phase with some of the harder secondary phase W_2C and a very small amount of metallic W
3	HIPed WC-12%Co/HVOF, Jet-kote	Powder: WC-12%Co (sintered and crushed, size: 15-50 µm), HIPed at 1123K, 150 MPa, 1 hr	300-325	0.047±0.03	1018±177	Main phase was primary WC, some eta-carbides (Co_6W_6C) formed by the interaction of the Co matrix and WC
Ceramic coatings						
4	Conventional Al_2O_3 (> 98% pure)/APS (Metco 9MB)	Powder: Al_2O_3 (angular and crushed, size: 10-45 µm), Arc current: 500 A, Arc voltage: 70 V, Primary gas: 37.6 l/min (Ar), Secondary gas: 7.1 l/min (H_2), Spray distance: 80 mm	250-260	0.27±0.02	683±38	γ-Al_2O_3 with some α -Al_2O_3
5	Fine powder Al_2O_3 (> 98% pure)/HVOF (Theta-gun)	Powder: Al_2O_3 (angular and crushed, size: 1-5 µm), Oxygen flow rate: 893 l/min, Kerosene flow rate: 0.32 l/min, Acetylene flow rate: 43 l/min, Spray distance: 150 mm	250-260	0.096±0.02	632±29	α -Al_2O_3 with very little γ-Al_2O_3

Table 2 Input parameters for finite element simulations.

Materials	**Elastic modulus, *E* (GPa)**	**Poisson's ratio, *v***	**Yield strength, σ_y (GPa)**	**Thickness (μm)**	**Ref. for *E* and *v***
Diamond indenter	1140	0.07	-	-	-
WC-12%Co coating	231	0.25	3.43	325	[28-29]
Substrate (AISI 440C Steel) for WC-12%Co coating	200	0.30	1.28	250	[28-29]
APS Al_2O_3 coating	130	0.23	2.23	260	[9]
Substrate (AISI 440C Steel) for APS Al_2O_3 coating	180	0.30	1.28	250	[9]
HVOF Al_2O_3 coating	170	0.23	2.06	260	[9]
Substrate (AISI 440C Steel) for HVOF Al_2O_3 coating	170	0.30	1.28	250	[9]

Table 3 Summary of qualitative and quantitative indentation cracking features.

Materials	**Indentation cracking type of surface** (ref. Fig. 4)	**Prevalence of radial cracking** (slope of line in m/N, ref. Fig. 5a)	**Prevalence of edge cracking** (slope of line in m/N, ref. Fig. 5b)	**Prevalence of total cracking** (slope of line in m/N, ref. Fig. 5b)
	Qualitative features	*Quantitative features*		
WC-12%Co (as-sprayed HVOF/JP5000)	Surface radial & edge cracks	2.04×10^{-7} (3^{rd} largest)	1.18×10^{-6} (3^{rd} largest)	1.80×10^{-6} (3^{rd} largest)
WC-12%Co (as-sprayed HVOF/JetKote)	Surface radial & edge cracks	2.60×10^{-7} (2^{nd} largest)	2.19×10^{-6} (2^{nd} largest)	2.79×10^{-6} (2^{nd} largest)
WC-12%Co (HIPed HVOF/JetKote)	Edge cracks	None	1.32×10^{-6} (4^{th} largest)	1.32×10^{-6} (4^{th} largest)
Conventional Al_2O_3 (APS/Metco, 9MB)	Spallation/ delamination	Not measurable	Not measurable	Not measurable
Fine powder Al_2O_3 (HVOF/theta gun)	Surface radial & edge cracks	4.09×10^{-7} (1^{st} largest)	2.48×10^{-6} (1^{st} largest)	4.12×10^{-6} (1^{st} largest)

Table 4 Summary of classical and alternative approach fracture toughness of coatings.

Materials	**Classical approach**	**Alternative approach**	
	Using average surface radial crack length, K_{1c} (MPa.m$^{1/2}$)	**Using total surface crack length,** K_{1c} (MPa.m$^{1/2}$)	**Using total surface crack length excluding total surface radial cracks,** K_{1c} (MPa.m$^{1/2}$)
As-sprayed HVOF (JetKote) WC-12%Co	8.81±0.47	4.6±0.3	5.2±0.3
As-sprayed HVOF (JP5000) WC-12%Co	9.07±1.02	7.1±0.1	7.4±0.5
HIPed HVOF (JetKote) WC-12%Co	No radial cracks	7.4±0.2	7.4±0.2
APS (Metco, 9MB) Al_2O_3 (conventional powder)	Cracks not measureable	Cracks not measureable	Cracks not measureable
HVOF (theta gun) Al_2O_3 (fine powder)	5.50±0.53	3.4±0.1	4.3±0.1

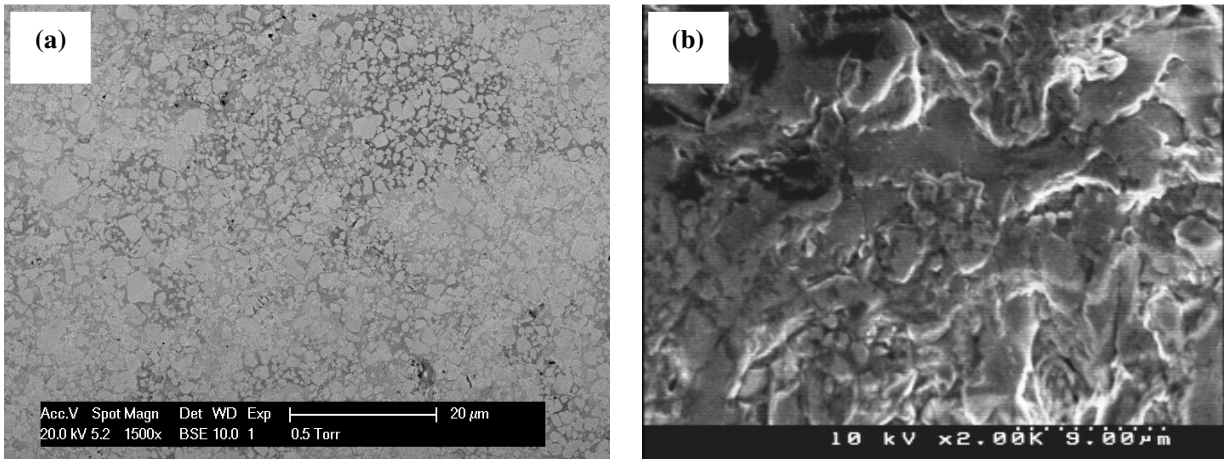

Fig. 1 SEM images of coatings surface morphology: (a) as-sprayed HVOF (JP5000) WC-12%Co. (b) APS (Metco/9 MB) Al_2O_3

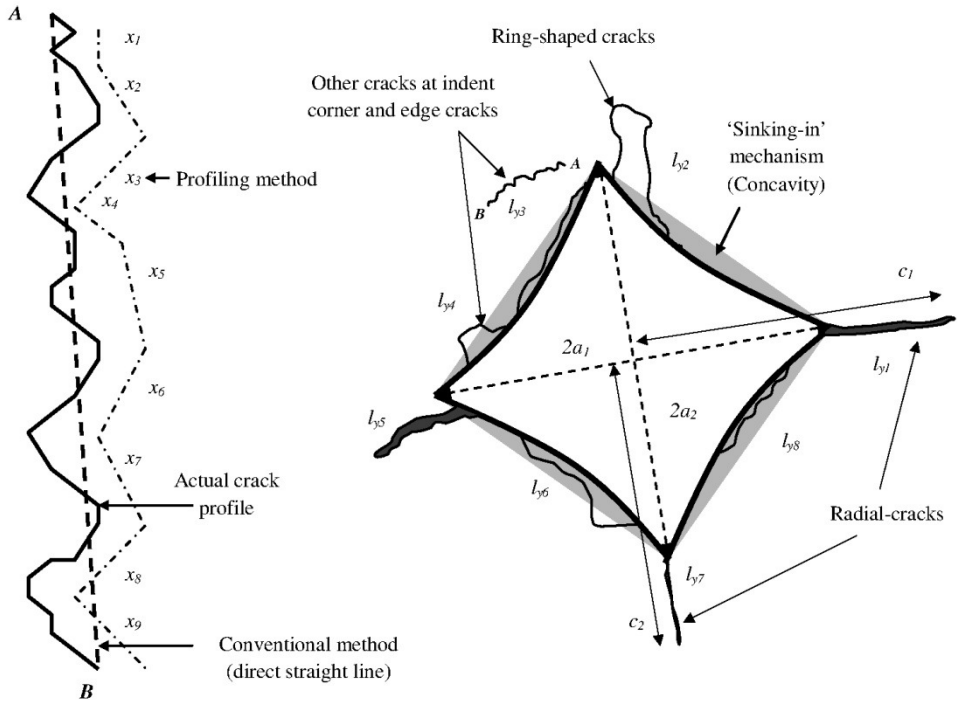

Fig. 2 Scheme for measuring the total surface crack length using profiling method. The scheme shown on the left side is applicable for all type of cracks around the indentation (ref. [12])

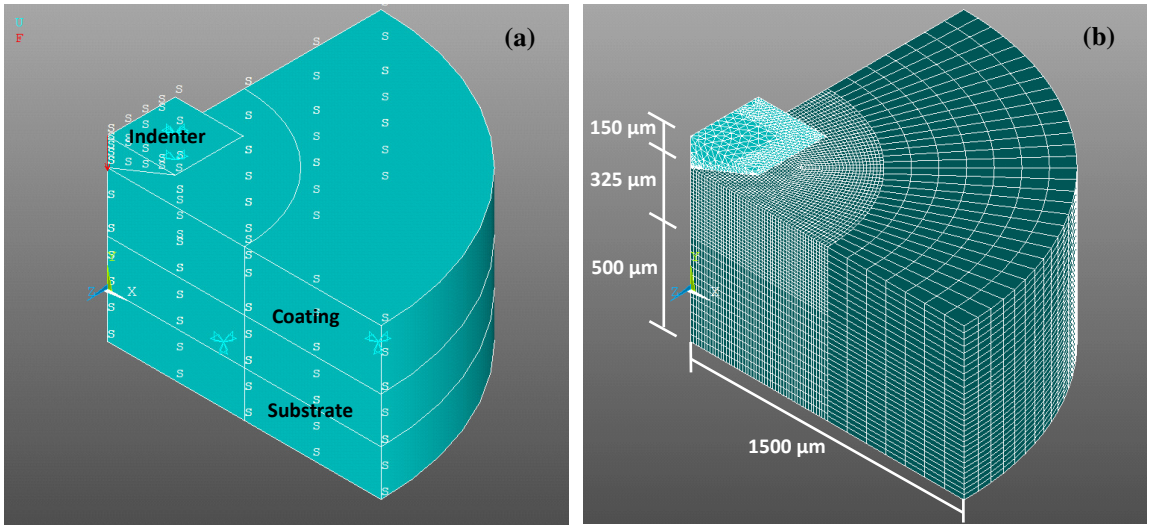

Fig. 3 Scheme for 3D elastic-plastic finite element modelling using ANSYS (14.0) Mechanical APDL: (a) constraints and loading conditions, and (b) meshing shown here for WC-12%Co coating on AISI 440C steel substrate

	(i) Vickers indentation (residual impression)	(ii) Schematic residual impressions	(iii) Key cracking features
(a)	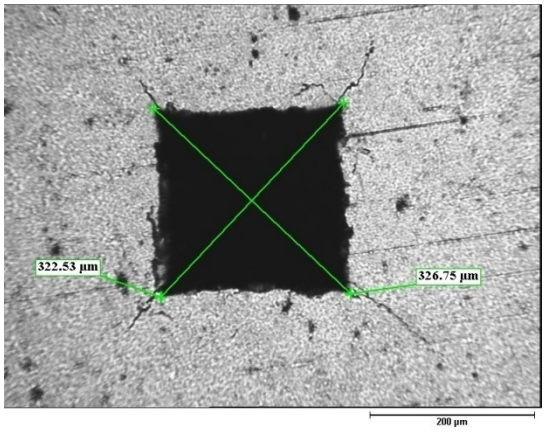	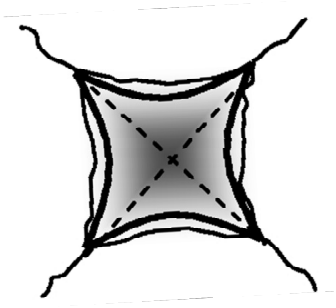	Surface radial & edge cracks
(b)	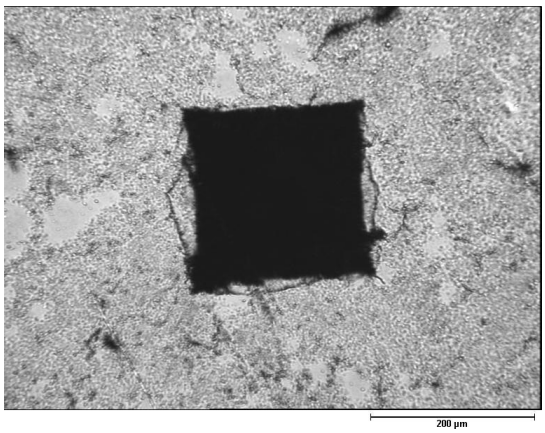	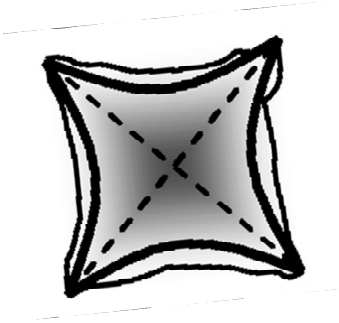	Edge cracks
(c)	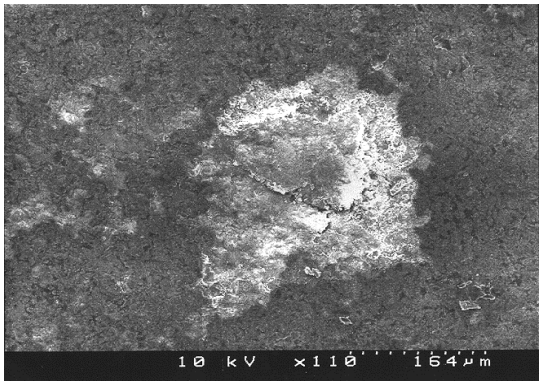	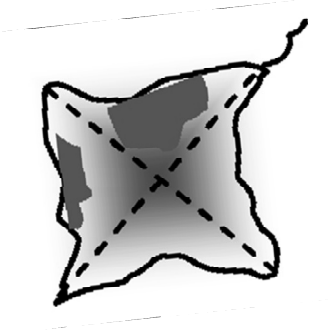	Spallation/delamination
(d)	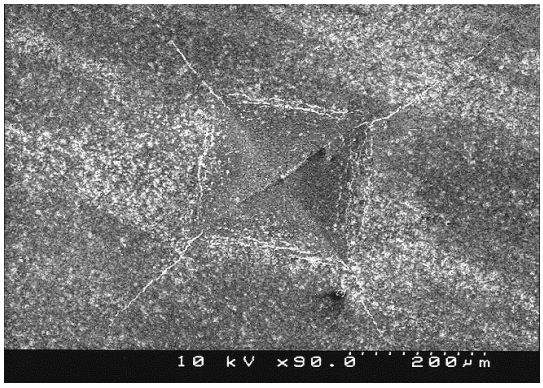	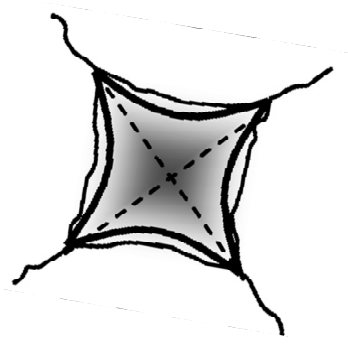	Surface radial & edge cracks

Fig. 4 Typical Vickers indentation cracking patterns of coatings at 441 N load: (a) as-sprayed (JP5000) WC-12%Co. (b) HIPed (JetKote) WC-12%Co. (c) APS (Metco/9 MB) Al_2O_3. (d) HVOF (theta-gun) Al_2O_3

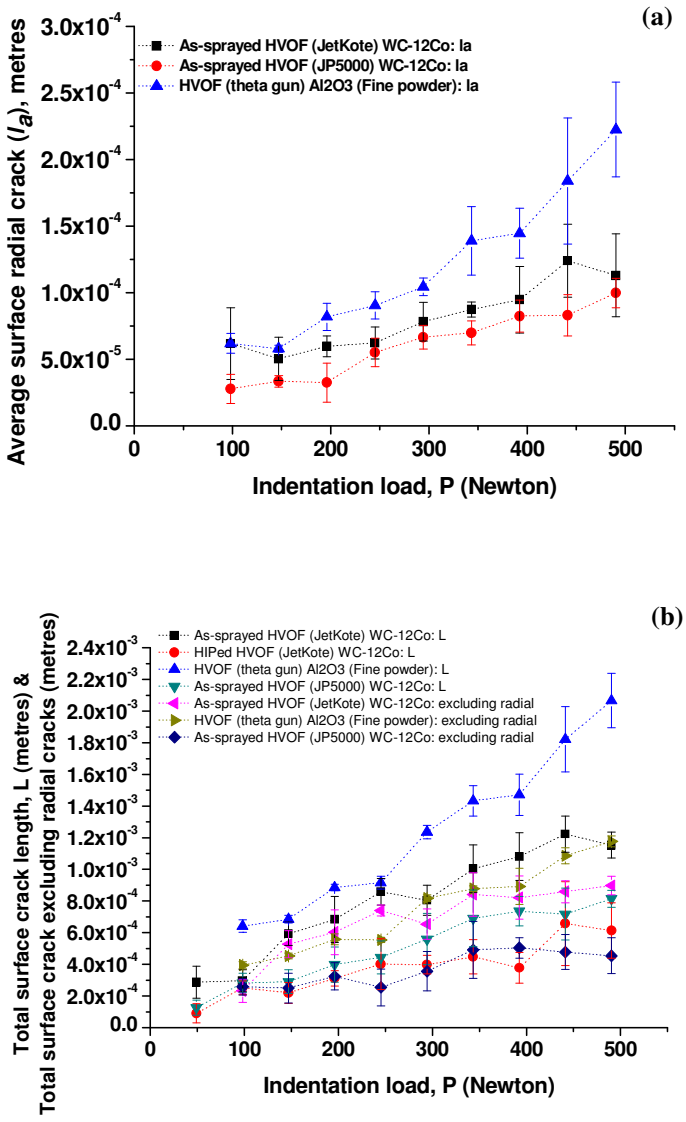

Fig. 5 Two approaches in Vickers indentation crack length indicator for fracture toughness assessment: (a) crack length indicator-1 (classical approach). (b) crack length indicator-2 (alternative approach). The error bars indicate the standard deviation of the data

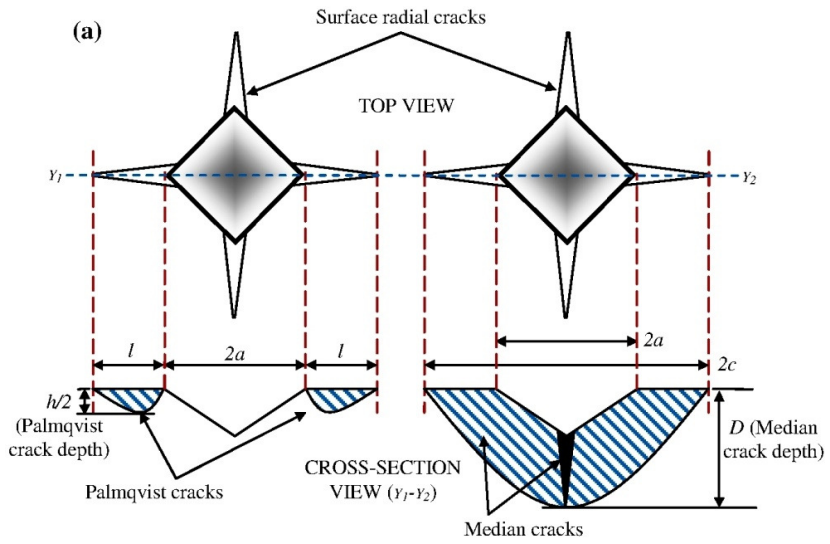

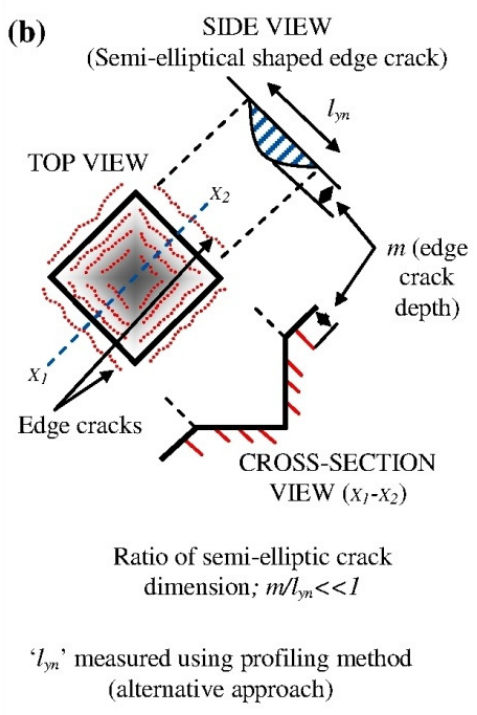

Fig. 6 Schematic diagrams of Vickers indentation residual impression for crack prone materials: (a) Plamqvist and half-penny models by Nihara [adapted from ref. 33] and Lawn and Fuller [adapted from ref. 34], and (b) edge crack model

(a) Crack length indicator-1

Average surface radial crack length (classical approach)

(b) Crack length indicator-2

Total surface crack length (alternative approach)

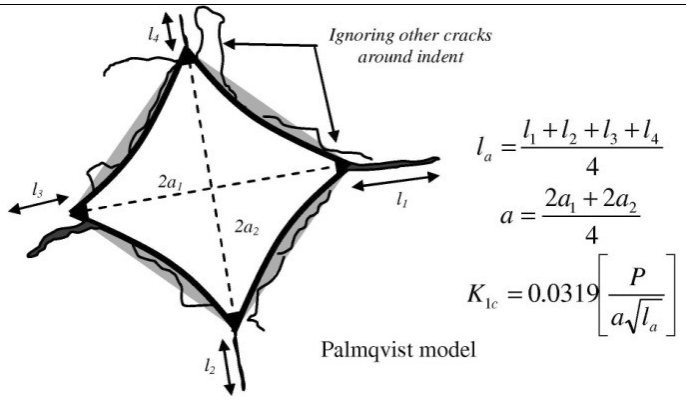

$$l_a = \frac{l_1 + l_2 + l_3 + l_4}{4}$$

$$a = \frac{2a_1 + 2a_2}{4}$$

$$K_{1c} = 0.0319\left[\frac{P}{a\sqrt{l_a}}\right]$$

$$L = \sum_n l_{yn}$$

$$K_{1c} = k_{total}\left[\frac{P}{a\sqrt{L}}\right]$$

$$k_{total} = 2\times 0.0319$$

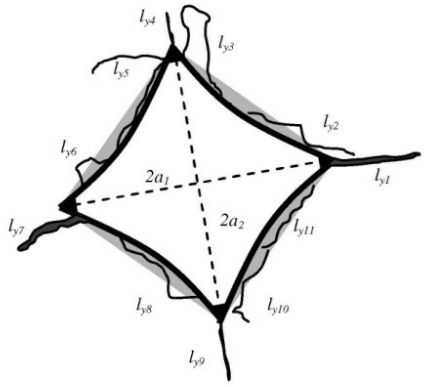

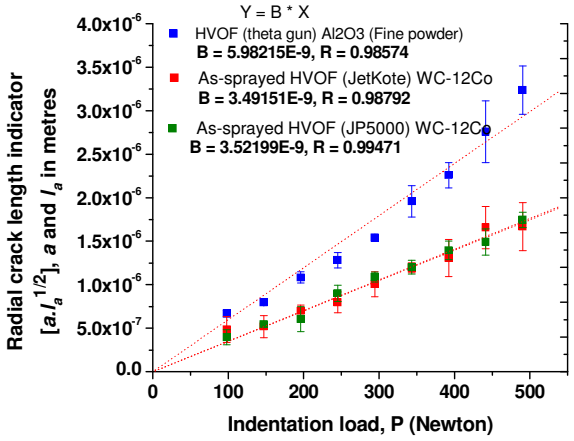

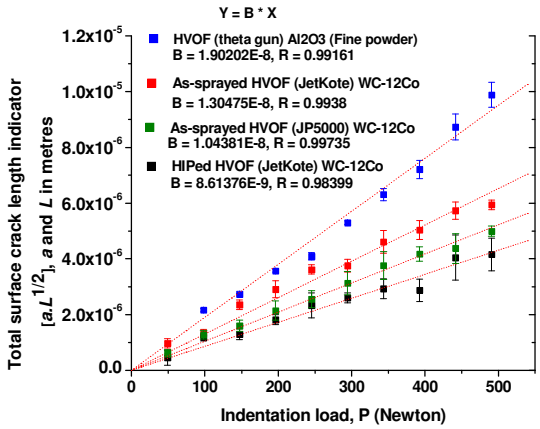

Fig. 7 Two approaches in Vickers indentation fracture toughness assessment: (a) crack length indicator-1 (classical approach). (b) crack length indicator-2 (alternative approach). The error bars indicate the standard deviation of the data

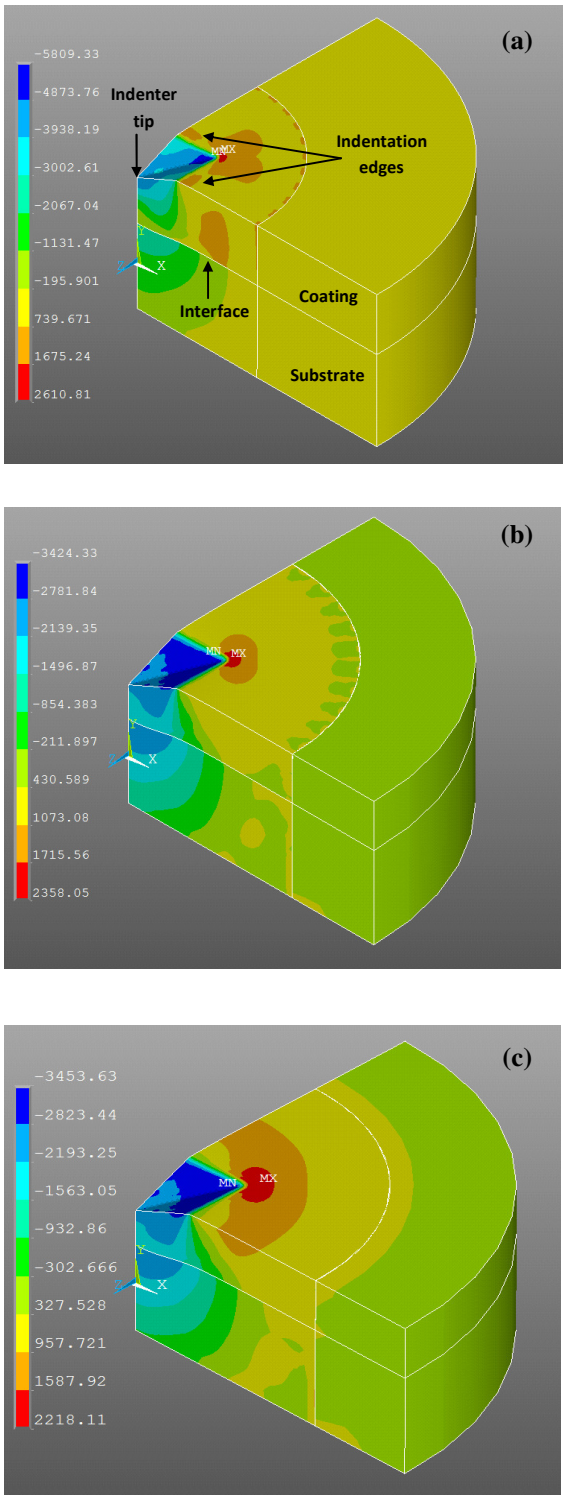

Fig. 8 Vickers indentation maximum principal stress at 490 N load for coatings: (a) WC-12%Co, (b) APS Al_2O_3, and (b) HVOF Al_2O_3 [Stress unit in MPa]

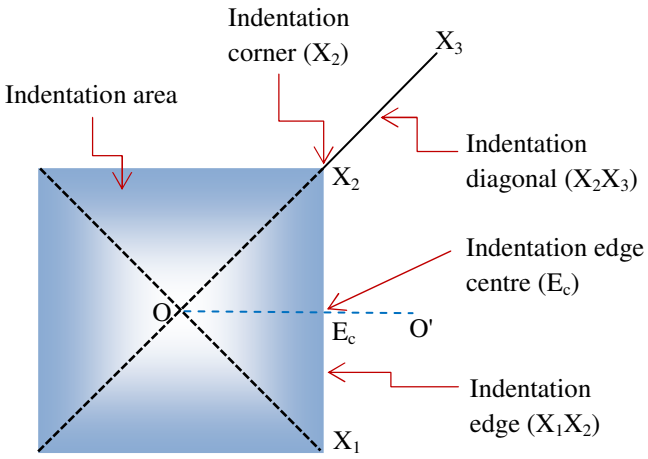

Fig. 9 Schematic of Vickers indentation impression (adapted from ref. [25])

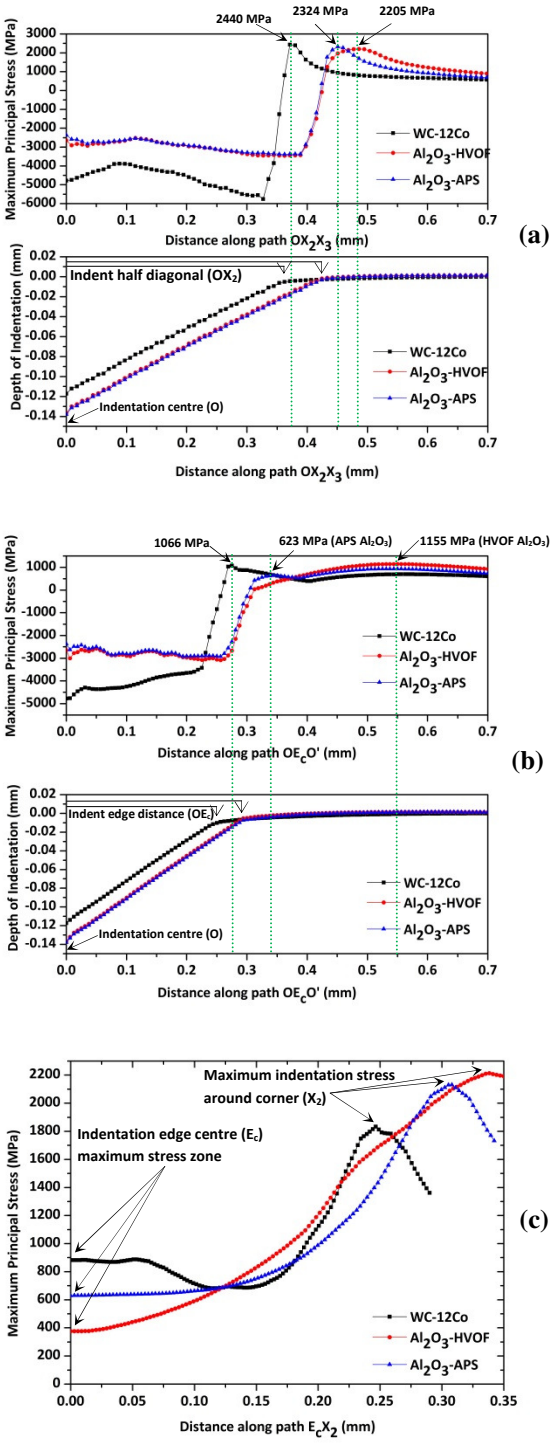

Fig. 10 Comparison and variation of the Vickers indentation maximum principal stress at 490 N load for coatings along various paths and depths: (a) path OX_2X_3, (b) OE_cO', and (c) E_cX_2